
Efficient Domain Adaptation of Multimodal embeddings using Contrastive Learning

Georgios Margaritis¹ Periklis Petridis¹ Dimitris J. Bertsimas²

Abstract

Recent advancements in machine learning (ML), natural language processing (NLP), and foundational models have shown promise for real-life applications in critical, albeit compute-constrained fields like healthcare. In such areas, combining foundational models with supervised ML offers potential for automating tasks like diagnosis and treatment planning, but the limited availability of onsite computational resources pose significant challenges before applying these technologies effectively: Current approaches either yield subpar results when using pretrained models without task-specific adaptation, or require substantial computational resources for fine-tuning, which is often a barrier to entry in such environments. This renders them inaccessible in applications where performance and quality standards are high, but computational resources are scarce. To bridge the gap between best-in-class performance and accessibility, we propose a novel method for adapting foundational, multimodal embeddings to downstream tasks, without the need of expensive fine-tuning processes. Our method leverages frozen embeddings from Large Language Models (LLMs) and Vision Models, and uses contrastive learning to train a small, task-specific nonlinear projection that can be used in the downstream task, without having to fine-tune the original foundational models. We show that this efficient procedure leads to significant performance improvements across various downstream tasks, and perhaps more importantly with minimal computational overhead, offering a practical solution for the use of advanced, foundational ML models in resource-constrained settings.

1. Introduction

Machine learning (ML) has grown very rapidly over the last 2 decades. This growth has inadvertently shown promise for its application in critical real-life applications, such as in clinical settings and healthcare operations. Although adoption of machine learning techniques in safety critical applications has had some inertia and initial skepticism, recent progress on safety, fairness, interpretability of ML models, as well as their performance, has created interest and momentum for their adoption from domain experts and practitioners. Now, with the advent of rapid progress in foundational models (FMs) and the demonstration of accessible, general purpose capabilities from recent large language models (LLMs) (Bubeck et al., 2023; Brown, 2020), the interest from practitioners has piqued. However, significant challenges still remain for the actual adoption of such models.

On the one hand, FMs like Llama (Dubey et al., 2024), BERT (Devlin et al., 2019), CLIP (Radford et al.), DINOv2 (Oquab et al., 2023), etc. can produce high quality embeddings from multiple modalities which offer great performance on complex downstream tasks. Hence, these models can be used out-of-the-box as feature extractors for various data types without the need for task-specific adaptation or fine-tuning (Soenksen et al., 2022). However, this approach often yields suboptimal results, as the resulting embeddings may be too general for specific tasks and frequently high-dimensional, potentially introducing noise in the classifier. Such performance limitations are particularly concerning in safety-critical applications like healthcare, where accuracy and reliability are necessary for real-world deployment.

On the other hand, fine-tuning these foundation models to adapt to specific downstream tasks is computationally demanding: It typically requires significant resources, such as large GPU servers and dedicated personnel, which are often missing from practical settings such as hospitals. To make matters worse, hospitals in particular, have to rely on the limited on-site computational resources, since sharing their sensitive data with third-party cloud providers is not an option. Hence, the cost and complexity of fine-tuning models with billions of parameters make it impractical or infeasible for most such real-world applications.

¹Operations Research Center, Massachusetts Institute of Technology ²Sloan School of Management, Massachusetts Institute of Technology. Correspondence to: Georgios Margaritis <geomar@mit.edu>, Periklis Petridis <periklis@mit.edu>.

As it stands currently, adoption of such models for practical assistance hinges on either (i) achieving very high model performance to satisfy the high standards of practitioners, which is often not feasible when using models without task-specific adaptation, or (ii) practitioners committing significant resources to build the necessary infrastructure to perform task-specific adaptation of the FMs. While this level of investment may occur in some instances, it severely limits the widespread adoption of such methods, especially in resource-constrained environments like many healthcare settings. This limitation creates a substantial barrier to leveraging the full potential of foundation models in critical real-world applications where they could provide the most benefit.

To tackle this problem, our approach offers an efficient way to adapt embeddings to a downstream task, without requiring the fine-tuning of foundation models. We propose an inexpensive, task-specific embedding adaptation process using contrastive learning which employs a nonlinear projection of the original embeddings into a lower-dimensional space, trained to bring embeddings with the same labels closer together while separating those with different labels. Our experiments on real-world clinical notes demonstrate significant improvements in performance, with increases in test F1 score of up to more than 20%, depending on the downstream model used. This approach provides a practical solution for leveraging the power of advanced ML models in resource-constrained settings, potentially facilitating wider adoption of these technologies in critical fields like healthcare.

Most contrastive learning methods require updating the entire embedding model in order to improve the quality of the embeddings. This process is computationally expensive, as it requires backpropagating the loss and updating the entire model, which can be costly both in terms of resources and time. Furthermore, many approaches also utilize implicit relationships between modalities, such as images and their captions, which may not be present in all multimodal settings. Instead, in our work, we develop a low-resource method that adapts to the task at hand efficiently, and only utilize the larger foundational models exactly once - to extract the initial embeddings. After this point, we train a small non-linear model to map the original embeddings to a new task-specific subspace using a contrastive objective, improving the quality of the embeddings for the task at hand. Then, we can use the transformed embedding for our downstream task.

Throughout this process, it is important to reiterate that the foundational model is not updated, and therefore the initial embeddings do not change as we train or modify our pipeline. This means we can run each of these large models for inference once on each modality, extract the

embeddings, and then simply store them for all future usage. As a matter of fact, the embeddings are potentially cheaper to store than the original raw data. Even if we modify our pipeline, adding or combining new modalities, or even if we want to adapt to a new task, we will not need to re-run the foundational models. After extracting the initial embeddings, our pipeline can run on a common CPU in less than a minute for thousands of samples.

To summarize, while our approach builds upon foundational contrastive learning methods, our contributions are the following:

1. We introduce a novel and computationally efficient method for task-specific adaptation of multimodal embeddings, which significantly improves embedding performance in downstream classification tasks. Our method uses contrastive learning to train a small nonlinear projection on top of frozen embeddings, and doesn't require fine-tuning of entire embedding models.
2. We test the effectiveness of our method for diagnosing health conditions from real-world clinical notes. Our experiments show that in most cases, our task-specific embeddings significantly outperform the original embeddings, increasing test F1 score by up to 20% or more, depending on the feature extractor and downstream ML model used. We also demonstrate that our results generalize to multiple ML models, multiple feature extractors and different multimodal datasets.
3. We show that our method has very low computational requirements, and can run in minutes in CPU-only settings. It thus makes the usage of foundational models more accessible in resource-constrained environments, such as healthcare settings. Additionally, our method can also reduce computational requirements by enabling label-aware dimensionality reduction, with performance significantly better than PCA.
4. Unlike conventional contrastive learning approaches tied to specific input types or implicit relationships (e.g. images and their captions), our method is modality-agnostic, since it operates on embeddings rather than raw inputs. This enables seamless integration of additional modalities using general-purpose embedding models, making it applicable across diverse data types and domains.

These contributions collectively offer a simple, efficient, and flexible approach to leveraging powerful foundation models in resource-constrained environments, addressing specific challenges in settings like healthcare where computational resources may be limited, data appears in various forms, and task-specific adaptation is crucial for accurate predictions.

2. Related Work

(Gutmann & Hyvärinen) laid out the groundwork for what is now contrastive learning by introducing Noise Contrastive Estimation (NCE) to estimate probabilistic models without computing partition functions. Word2Vec (Mikolov, 2013) was one of the early applications of NCE in Natural Language Processing (NLP) and also introduced negative sampling to train word embeddings efficiently. More recent developments using contrastive learning have led to significant advancements in representation learning.

Contrastive Learning in Vision. Notably, most of the recent work in this area has focused on unsupervised visual representation learning by utilizing data augmentations. For instance, SimCLR (Chen et al.) utilizes contrastive learning with data augmentation to learn visual representations. SwAV (Caron et al.) combines clustering with contrastive learning for unsupervised visual representation learning. MoCo (He et al.) introduces a momentum contrast mechanism for unsupervised visual representation learning. In contrast, our method focuses on supervised tasks and uses task labels to adapt embeddings to the downstream task.

Contrastive Learning in Multimodal Settings. In multimodal settings, contrastive learning has been used to learn joint representations of different modalities, typically images and text, by utilizing an implicit relationship, say images and their captions. One of the first major works is Contrastive Predictive Coding (CPC) (Oord et al.) which introduces a way to learn representations by predicting future observations in latent space. Another notable work is CLIP (Radford et al., 2021) which learns joint representations of images and text by pre-training on a large dataset of image-caption pairs. Other examples include ConVIRT (Zhang et al.) which applies contrastive learning to medical imaging by leveraging text reports associated with images and ALIGN (Jia et al.), which scales up visual and vision-language representation learning with noisy text supervision. However, these methods are designed for specific input types and rely on an implicit relationship between modalities, which may not be present in all multimodal settings. Our method is modality-agnostic and can be applied to any modality or combination thereof, as long as we have a general-purpose embedding model that can process that modality.

Contrastive Learning in Clinical Settings. A ripe area for application of contrastive learning techniques is in clinical settings, where we frequently have multimodal data. To this end, ConVIRT (Zhang et al.) applies contrastive learning to medical imaging by leveraging radiology reports associated with x-ray images. A different approach is (Xia et al.), which utilizes contrastive learning to improve representations of MLP and encoder architectures with partially missing sources for patients’ tabular data. However,

the above methods are again constrained by the structure of the data or its implicit relationships. Our approach can utilize any type of data, and can be applied to any binary classification task.

3. Methodology

In this section we outline how we implement Contrastive Learning to perform task-specific embedding adaptation. We first outline the problem setting, and then we analyze our Contrastive Learning approach.

3.1. Problem Setting

Consider the problem of binary classification based on multimodal data, where we have data from m different sources/modalities.

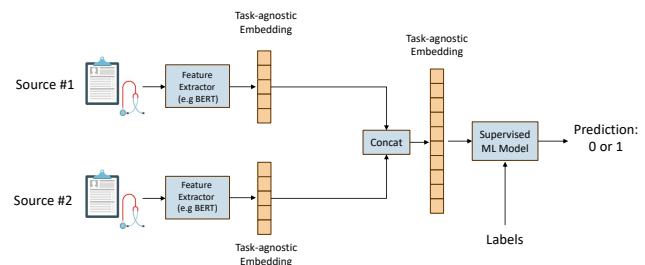


Figure 1: Multimodal prediction with task-agnostic embeddings

A typical approach to address this problem is to use a feature extractor to generate features/embeddings from every source, and then fuse all the features and then train a supervised ML model to predict the desired class from the fused features. For instance, in the clinical setting, we may have textual data from clinical notes, images from radiology scans, and structured data from lab results, and we want to predict a binary label (e.g. disease vs. no disease) based on these multimodal data sources. This pipeline is illustrated in Figure (1) and has been successfully applied in large-scale multimodal clinical data, as shown in (Soenksen et al., 2022).

In this setting, each source embedding can be generated using a different feature extractor, depending on the nature of the data source. For instance, extracting embeddings from textual sources can be done with BERT (Devlin et al., 2019), Llama3 combined with LLM2Vec (Dubey et al., 2024; BehnamGhader et al., 2024) or Qwen2 combined with GTE (Yang et al., 2024; Li et al., 2023). For visual sources, we can use models like DINOv2 (Oquab et al., 2024), Vision Transformers (ViT) (Dosovitskiy, 2020), CLIP (Radford et al.), and others.

In all of these cases, we can find publicly-available versions of these models that we can use to extract embeddings without training these architectures from scratch. This is particularly useful in scenarios where we have limited computational resources and we cannot resort to expensive task-specific training or finetuning procedures (such as using Masked Language Modeling to adapt large-scale LLMs to our task). For instance, in most real-world applications, training, or even fine-tuning an LLM with billions of parameters to a specific task can be extremely costly, impractical or even infeasible.

However, task-agnostic embedding generation can have serious drawbacks. Using pre-trained feature extractors without any form of finetuning to the downstream task produces general-purpose and task-agnostic embeddings. These embeddings may perform poorly in the specific downstream task. At the same time, such embeddings can also be very high-dimensional (e.g. 4096 for Llama3), which may introduce a lot of noise in the resulting classifier.

To mitigate both of these issues, we propose an inexpensive way of creating task-specific embeddings, which in turn demonstrate significantly better performance than the task-agnostic embeddings in the binary classification task. Our method uses an inexpensive nonlinear projection of the original embeddings into a lower-dimensional space. This nonlinear projection is trained using Contrastive Learning, such that the output vectors of the projection that correspond to the same binary labels are close to one another, and the output vectors that correspond to different labels are far from one another.

3.2. Approach

In this section, we describe our approach for task-specific embedding adaptation.

Assume we have n data points and for each data point $i \in [n]$ we have task-agnostic embeddings $e_i^{(1)}, \dots, e_i^{(m)}$, where m corresponds to the number of modalities. For each data point, we also have a label y_i which we assume to be binary.

Let $f(x) : \mathbb{R}^M \rightarrow \mathbb{R}^K$ with $K < M$ be a dimension-reducing nonlinear projection. We consider 2 different projection paradigms which are shown in Figure (2):

- **Single Projection:** The embeddings are concatenated into a single embedding $e_i = [e_i^{(1)}, \dots, e_i^{(m)}]$ and the resulting vector is passed from the projection as $p_i = f(e_i)$. Then, we use the projected embedding p_i in our downstream task (Figure 2a).
- **Per-modality Projection:** Each embedding modality is projected using a different projec-

tion $p_i^{(j)} = f_j(e_i^{(j)})$, $j \in [m]$, and the projections are then concatenated into a vector $p = [p_i^{(1)}, \dots, p_i^{(m)}]$. This vector is used in our downstream task (Figure 2b).

In both cases, we consider f and f_j to be small feed-forward ReLU NN projections, and we use the labels y_i to train these projections using Contrastive Learning.

To analyze the method, we will focus on the per-modality projection case, since the single-projection case is a simpler extension of this. In that setting, let's focus on the projection of a single modality $p_i^{(j)} = f_j(e_i^{(j)})$. To train our projection, we first get a random minibatch of size B from the original dataset, which we assume without loss of generality that it contains the tuples $(e_1^{(j)}, y_1), \dots, (e_B^{(j)}, y_B)$. We then construct the following dataset of constrastive pairs:

$$C_b^{(j)} = \{ (e_i^{(j)}, e_k^{(j)}, \mathbb{1}\{y_i = y_k\}) \}_{k \leq i, i \in [B]} \quad (1)$$

For this batch, we calculate the following contrastive loss, which is similar to the SimCLR loss of (Chen et al.):

$$\mathcal{L}_b^{(j)} = - \sum_{(u, v, \ell) \in C_b^{(j)}} \left[\ell \cdot \log \sigma(g_j^T(u)g_j(v)/\tau) + (1 - \ell) \cdot \log \sigma(g_j^T(u)g_j(v)/\tau) \right]. \quad (2)$$

We repeat the process for the remaining minibatches of the original dataset, and we use this loss to train our nonlinear projection f_j . If we are using per-modality projections, then each projection is trained independently from the others. If we are using a single projection, then the projection is trained exactly the same way, but in this case, the input of f is not a single-modality embedding e_j , but rather the concatenated embeddings $[e_i^{(1)}, \dots, e_i^{(m)}]$.

Note that the loss $\mathcal{L}_b^{(j)}$ corresponds to a binary, cross-entropy loss with sigmoid activation. Here our logit is $g_j^T(u)g_j(v)/\tau$ which is the similarity of the 2 projections u and v divided by a temperature constant τ . Also, our label is 1 iff both embeddings u and v correspond to the same label. Intuitively, we want to learn a projection function f_j such that embeddings corresponding to the same label will have a similar projections and embeddings corresponding to different labels will have different projections.

After training the projection(s), we use them to project our original embeddings and generate a task-specific embeddings for each data-point. Then, we use these new embeddings, together with the labels y_i , to train a binary classification model. This process is illustrated in Figure (2).

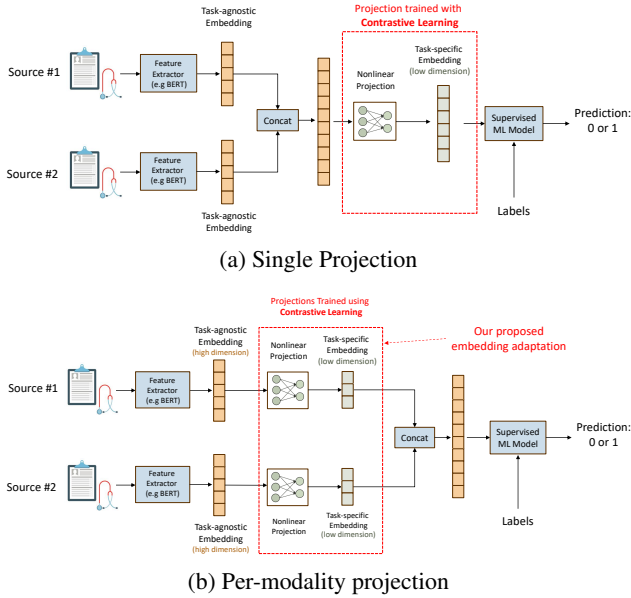


Figure 2: Multimodal prediction with task-specific embeddings

3.3. Datasets & Feature Extractors

In order to evaluate our approach, we use 2 different datasets: A proprietary healthcare dataset from our ongoing collaboration with Hartford Healthcare Hospital System (HHC), and a publicly-available multimodal movie dataset. Below we describe these datasets and the ways that we preprocessed them. We also outline the embedding-extractors we use for each dataset.

3.3.1. HEALTHCARE DATA

Through our IRB-approved research protocol, we have access to Electronic Health Records (EHRs) of 4000 patients from the EPIC database of HHC, which is a centralized clinical data registry that contains information on patient demographics, medical problems, laboratory data, and various clinical notes and documents. From these records, we utilize the following distinct sources of data:

1. The **History & Physical (H&P)**, which is a clinical note that contains information about current and past conditions of the patient, risk factors, past medications, and other essential information that aids physicians to determine the individual’s health status.
2. The **Progress Note (Prg)**, which describes the patient’s condition and treatment plan, and documents their progress or lack thereof between the previous and the most recent note.
3. The **ICD-9/ICD-10 diagnosis codes**, which are stan-

dardized diagnostic codes used for clinical classification and billing purposes.

We treat these sources as 3 independent data sources/modalities. The first 2 sources are textual, and can be passed directly from a language model to generate embeddings. For the 3rd source, we first convert the International Classification of Diseases (ICD-9/ICD-10) codes into human-readable diagnoses texts using established mapping tables (Healthcare Cost and Utilization Project (HCUP), 2021). This process of converting structured, tabular information into text has been shown to yield better performance than using the data as structured features (Carballo et al., 2023). Then, we can also pass this text representation from a language model to extract embeddings.

For each patient, we also have binary labels about the existence of various health conditions, such as diabetes, hypertension, chronic lung disease, and others. Hence, given these labels, our supervised ML task is to predict the existence of the various conditions from the 3 clinical sources we described. In particular, in this work, we focus on predicting diabetes and hypertension from the EHR sources.

For this dataset, we use 2 different feature extractors to generate embeddings from the text sources. We first use ClinicalBERT (Huang et al., 2019), which has been used extensively for embedding extraction in Healthcare applications (e.g. see (Soenksen et al., 2022)). Secondly, we also wanted to try a more recent large-scale language model. For this reason, we opted for Qwen2 (Yang et al., 2024) with 7B parameters, which is an open-source conversational model produced by Alibaba group. However, since decoder-only models are not good for producing high-quality embeddings out of the box (i.e. due to their causal attention mask, (BehnamGhader et al., 2024)), we use the GTE-pretrained version of Qwen2 ((Li et al., 2023)), which adapts Qwen2 for embedding generation. Note that the reason we opted for using Qwen2 instead of Llama3, is because Qwen2 with GTE pretraining ranks among the top models in the Massive Text Embedding benchmark (MTEB, (Muennighoff et al., 2023)).

3.3.2. MULTIMODAL MOVIE DATASET

As our second dataset, we use *mmimdb* (Arevalo et al., 2017), which is the largest publicly-available multimodal dataset for movie genre prediction. From this dataset, we utilize the *image*, *title*, *year*, *rating* and the *plot summary* of the movie as our input data, which we use to predict whether a movie is a comedy or a drama (i.e. binary classification). In particular, for each movie, we first generate a single piece of text which contains all the tabular information we mentioned. An example is shown in Figure (3).

Title: Titanic
Country: United States
Plot: A seventeen-year-old aristocrat, expecting to be married to a wealthy suitor, falls in love with a kind but poor artist aboard the luxurious, ill-fated R.M.S. Titanic.
Rating: 7.9
Year: 1997

Figure 3: Tabular movie information as a single text

Using this approach, we convert the movie’s tabular information into text, and thus the data can now be parsed by an LLM, similar to (Carballo et al., 2023). We also use the movie poster image as a separate modality. Hence, we now have a single text modality and a single image modality for our predictive task.

Finally, as for the labels, we only keep movies that belong to either the Comedy genre or the Drama genre (those were the most populous classes in our dataset). This way, we end up with a binary classification task with 3606 datapoints.

Finally, for the feature-extraction step, we use a different pretrained model to generate embeddings from images and a different model to generate embeddings from text. For images, we use a Vision Transformer (ViT-16, (Dosovitskiy et al., 2021)) which is pretrained on the Imagenet dataset. For text, we use a standard BERT model (Devlin et al., 2019). Note that here we don’t use the clinical version of BERT, since our application is non medical.

4. Results

In this section, we evaluate our approach in the 2 datasets we described. We perform this comparison for different feature extractors and downstream models, and we show that in the majority of cases, our projection method offers significant improvements compared to the other methods.

For our evaluation, we first use pretrained feature-extractors to generate task-agnostic embeddings for the different data modalities, as mentioned in Sections 3.3.1 and 3.3.2. Then, we test 3 different approaches for performing supervised classification using the extracted embeddings:

- **Unprojected:** We fuse the embeddings from the different modalities together through simple concatenation. Then, we use a standard supervised ML model to predict the target label given the fused embeddings.
- **Contrastive:** We first project the embeddings into a lower-dimensional space using the approach described in Section 3.2. Then, we use the resulting embeddings to perform supervised classification.
- **PCA:** We project the embeddings into a lower dimensional space using PCA, and then we use the projected

Table 1: Contrastive learning hyperparameters

HYPERPARAMETER	MEDICAL	MOVIES
LEARNING RATE (γ)	10^{-3}	10^{-3}
MINIBATCH SIZE (B)	128	128
NUMBER OF EPOCHS (N)	10	15
TEMPERATURE (τ)	0.1	0.1
PROJECTION HIDDEN LAYERS	1	1
PROJECTION SIZE	128	128

embeddings for classification.

For the projection approaches (i.e. PCA and Contrastive projection), we experiment with (i) Performing a single projection of the original, concatenated embeddings and (ii) Performing a different projection for each modality and concatenating the embeddings afterwards. The 2 approaches are illustrated in Figures (2a) and (2b) respectively.

For both PCA and the Contrastive projection, we use a projection size of 128. Then, in order to train the Contrastive projections, we use the hyperparameters shown in Table (1).

After projecting the embeddings with the different approaches, we use the embeddings in a binary classification task using RandomForest, XGBoost, CART, Logistic Regression, Support Vector Classifiers with RBF kernel and Multi-layer perceptrons with ReLU activations (MLP). For all models, we use the default parameters and we don’t perform hyperparameter tuning, in order to ensure fairness in our evaluation. For comparing the different methods, we measure average out-of-sample F1 score using 5-fold cross validation. We have also included detailed F1, ROC AUC and Accuracy results in Appendix A.

Table 2: Average F1 Score (%) Across Experiments

METHOD	DIABETES	HYPERTENSION	MOVIES
UNPROJECTED	58.3 (± 23.5)	19.8 (± 13.9)	56.2 (± 27.3)
SINGLE PROJ (CONTR.)	59.9 (± 27.6)	23.7 (± 10.8)	64.7 (± 24.8)
SINGLE PROJ (PCA)	52.5 (± 25.9)	17.1 (± 10.9)	58.7 (± 27.8)
PER-MOD (CONTR.)	76.3 (± 5.4)	27.6 (± 6.3)	76.4 (± 2.4)
PER-MOD (PCA)	55.7 (± 27.3)	20.6 (± 13.4)	54.5 (± 28.1)

VALUES SHOW MEAN F1 SCORES & STANDARD DEVIATIONS ACROSS ALL MODELS AND FEATURE EXTRACTORS

Table (2) shows the average performance of each projection method for each task (Diabetes, Hypertension, Movies). We then proceed to analyze in detail the different tasks and the individual results.

4.1. Medical Dataset

For the medical dataset, we test the models on predicting diabetes and hypertension. The results are shown in Tables (3) and (4) respectively.

Table 3: $\Delta F1$ score (%) for *diabetes* with each projection method. Values show differences from unprojected baseline. Best results are shown in **bold**.

EXTR.	MODEL	SINGLE PROJ.		PER-MOD. PROJ.	
		CONTR.	PCA	CONTR.	PCA
CBERT	CART	+18.2 (± 3.2)	-7.3 (± 1.9)	+18.3 (± 2.0)	-3.6 (± 2.7)
CBERT	LR	-2.7 (± 1.9)	-2.1 (± 1.0)	+0.1 (± 1.9)	-1.1 (± 1.6)
CBERT	MLP	-2.0 (± 1.6)	-4.2 (± 1.7)	+1.5 (± 2.2)	+0.1 (± 1.3)
CBERT	SVC	+9.6 (± 4.9)	+0.0 (± 0.0)	+81.2 (± 1.9)	+0.0 (± 0.0)
CBERT	XGB	+4.1 (± 1.9)	-7.1 (± 2.1)	+7.0 (± 2.6)	-1.6 (± 2.1)
GQW	CART	+15.7 (± 2.5)	-0.9 (± 0.9)	+21.0 (± 0.9)	+1.3 (± 2.0)
GQW	LR	+6.2 (± 0.8)	+5.4 (± 1.3)	+12.2 (± 1.3)	+9.9 (± 1.4)
GQW	MLP	-3.5 (± 1.3)	-5.9 (± 1.7)	+3.1 (± 1.4)	-1.2 (± 1.5)
GQW	SVC	-26.6 (± 0.0)	-26.6 (± 0.0)	+43.9 (± 0.9)	-26.6 (± 0.0)
GQW	XGB	+6.2 (± 2.2)	-6.9 (± 1.3)	+12.9 (± 1.8)	+0.5 (± 1.3)

EXTRACTORS – CBERT: CLINICALBERT, GQW: GTE+QWEN2
 MODELS – LR: LOG. REGRESSION, RF: RANDOM FOREST

Table 4: $\Delta F1$ score (%) for *hypertension* with each projection method. Values show differences from unprojected baseline. Best results are shown in **bold**.

EXTR.	MODEL	SINGLE PROJ.		PER-MOD. PROJ.	
		CONTR.	PCA	CONTR.	PCA
CBERT	CART	+3.6 (± 4.4)	-2.7 (± 2.9)	+3.4 (± 3.8)	+0.0 (± 1.9)
CBERT	LR	-4.5 (± 3.7)	-9.9 (± 4.3)	-6.2 (± 3.1)	+1.1 (± 3.8)
CBERT	MLP	-4.1 (± 5.2)	-3.1 (± 3.1)	-2.7 (± 2.1)	+2.5 (± 4.7)
CBERT	SVC	+11.0 (± 3.5)	+0.0 (± 0.0)	+19.5 (± 4.6)	+0.0 (± 0.0)
CBERT	XGB	+9.3 (± 4.3)	-9.0 (± 4.1)	+8.0 (± 4.7)	-5.8 (± 3.7)
GQW	CART	+7.0 (± 2.7)	+4.0 (± 1.9)	+13.0 (± 5.9)	+5.1 (± 4.2)
GQW	LR	+26.5 (± 4.1)	+10.9 (± 3.3)	+21.8 (± 2.7)	+24.3 (± 2.9)
GQW	MLP	-1.7 (± 3.7)	-2.3 (± 3.1)	-7.3 (± 5.9)	-1.8 (± 3.9)
GQW	SVC	+0.0 (± 0.0)	+0.0 (± 0.0)	+8.5 (± 4.7)	+0.0 (± 0.0)
GQW	XGB	+19.9 (± 3.5)	-0.7 (± 1.9)	+16.6 (± 5.8)	+0.7 (± 3.0)

EXTRACTORS – CBERT: CLINICALBERT, GQW: GTE+QWEN2
 MODELS – LR: LOG. REGRESSION, RF: RANDOM FOREST

Examining the results for predicting *diabetes* (Table (3)) and *hypertension* (Table (4)), we can see than in the vast majority of cases, our contrastive projections beat both the unprojected embeddings and the embeddings projected using PCA. In fact, for many combination of models and feature extractors, our method beats the baseline by more than 10% in terms of F1 score, demonstrating significant improvement at a very low computational cost.

To better understand this behavior, we focus on the task of predicting *diabetes* using a single projection, and we perform a t-SNE visualization of the embeddings before and after the contrastive projection. We also indicate the labels with a different color (i.e. blue indicates no diabetes and red indicates diabetes), as shown in Figure (4). From this figure, it is evident that before the projection, there doesn't seem to be a clear class separation, but after the contrastive projection, the label separation becomes very pronounced. This explains why simpler ML models (i.e. models with simpler decision boundaries) such as SVC and CART tend to perform much better when applied to the projected embeddings rather than the original embeddings.

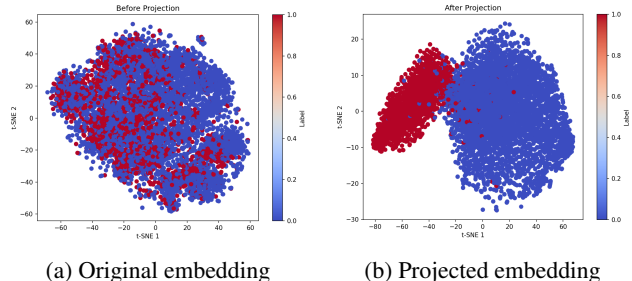


Figure 4: t-SNE plot of embeddings before and after contrastive projection.

4.2. Movie Dataset

For the multimodal movie-genre prediction dataset, our downstream task was to predict whether the movie is comedy or drama. The results are shown on Table (5).

Table 5: $\Delta F1$ score (%) for *movies* with each projection method. Values show differences from unprojected baseline. Best results are shown in **bold**.

EXTR.	MODEL	SINGLE PROJ.		PER-MOD. PROJ.	
		CONTR.	PCA	CONTR.	PCA
BViT	CART	+19.5 (± 2.7)	+4.6 (± 2.5)	+19.6 (± 1.7)	-2.5 (± 1.7)
BViT	LR	-0.4 (± 1.6)	+2.2 (± 1.3)	-0.7 (± 2.4)	+1.7 (± 1.9)
BViT	MLP	-2.0 (± 1.0)	+0.6 (± 1.2)	-1.5 (± 3.3)	+0.8 (± 1.9)
BViT	RF	+20.3 (± 2.3)	+4.6 (± 4.5)	+20.1 (± 2.6)	-14.8 (± 2.7)
BViT	SVC	+30.3 (± 16.0)	+0.0 (± 0.4)	+75.1 (± 2.7)	-0.3 (± 0.0)
BViT	XGB	+3.4 (± 2.5)	+2.8 (± 2.2)	+4.3 (± 1.9)	-0.8 (± 1.8)

EXTRACTORS – BViT: BERT+ViT MULTIMODAL MODEL
 MODELS – LR: LOG. REGRESSION, RF: RANDOM FOREST

We can see than in 3 out of the 5 cases, our contrastive projection outperforms the other methods by a significant margin. These results are consistent with the medical dataset, showing that depending on the downstream model used, the contrastive projection has the potential to offer significant performance improvements compared to conventional methods.

4.3. Time-Performance Trade-off

In the previous sections, we established that our method can have significant performance benefits in various downstream tasks. In this section, we show that the computational overhead it introduces is negligible, maintaining roughly the same execution time and resources as the unprojected baseline. To further showcase the utility our method, we also compare the performance and resources it uses against a scenario where the feature extractors of the different sources are fully fine-tuned to the downstream task. We then show that fine-tuning the feature extractors, despite having better downstream performance, is orders of mag-

nitude slower than our method, making it inaccessible in resource-constrained environments.

For the timing benchmarks, we focus on the task of predicting diabetes from the 3 sources of the Medical Dataset. We use ClinicalBERT as the feature extractor for all sources, and we use MLP as our downstream model, so that the entire architecture (including the feature extractors) can be fine-tuned using backpropagation. We test 3 different downstream training paradigms:

1. **Unprojected Baseline:** Same as the baseline used in previous sections (Figure (1)), where MLP is the downstream model and feature-extractors are kept frozen.
2. **Contrastive Per-modality projection:** Each modality is projected independently, and the projections are trained through Contrastive Learning (Figure (2b)). MLP is used as the downstream model and feature-extractors are kept frozen.
3. **Full Finetuning:** The initial embeddings are concatenated and a classification head is added on top of them. Then, the entire architecture (including the ClinicalBERT feature extractors) is trained/finetuned to predict diabetes. A small number of epochs ($e = 5$) is used to prevent catastrophic forgetting.

For each of the methods, we run experiments (i) using only CPU and (ii) using both CPU and GPU. The CPU and GPU used is an Intel(R) Xeon(R) Silver 4316 CPU @ 2.30GHz and an 80GB NVIDIA A100 GPU. When using the CPU, we are only utilizing 8 cores to emulate performance of a real-world resource-constrained scenario.

Due to high computational demands, and in order to ensure fairness, we run a single experiment from each type. In each of our experiments, we measure F1 score, training time and VRAM. The results are reported in Table (6). We also construct a time-performance trade-off plot (Figure (5)).

Comparing the different approaches, it is clear that our Contrastive approach has a very similar execution time as the unprojected baseline, both in the CPU and in the CPU+GPU scenario. In fact, it is clear that our method doesn't even require a GPU, since it can run in less than a minute for $\sim 4k$ datapoints in a conventional CPU. However, despite its low computational footprint, our method still offers a 3% improvement in diagnostic quality in terms of F1-score.

On the other hand, fine-tuning the feature extractors does indeed offer a 6% better performance than our method, albeit at a much higher computational cost. In fact, running the full fine-tuning procedure takes 3 orders of more time (i.e. around 11 hours) and requires a powerful GPU with more than 32 GB of VRAM, resources which are rarely found in real-world hospital settings. At the same time, it is evident

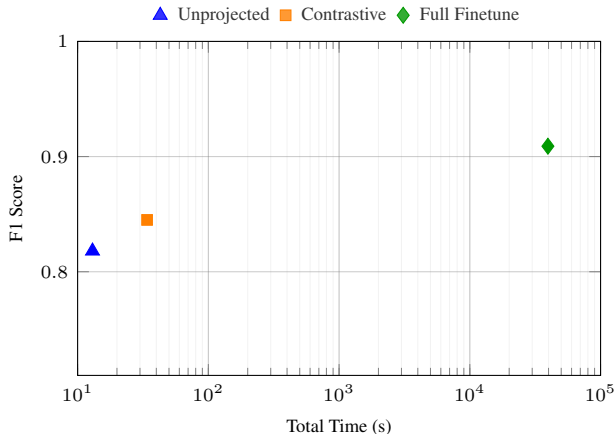


Figure 5: Time-performance trade-off

that such fine-tuning methods are completely inapplicable in CPU-only environments.

Table 6: Performance & Time of the different methods

METHOD	F1	RESOURCE		
		CPU	GPU	
		TIME (S)	TIME (S)	VRAM (MB)
UNPROJECTED	0.818	14	13	–
CONTRASTIVE	0.845	51	34	3
FULL FINETUNE	0.909	–	39562	33770

TIME MEASURED ON 80GB NVIDIA A100 GPU / INTEL(R) XEON(R) SILVER 4316 CPU @ 2.30GHZ

5. Conclusion

We introduced a general-purpose method that utilizes contrastive learning to learn a downstream task-specific non-linear projection to improve the performance of the prediction head. Our method runs in minutes, is low-resource, and offers significant improvements, without having to resort to expensive fine-tuning processes of foundation models. Furthermore, it's flexible, allowing for any multimodal combination, and can be applied for any binary classification downstream task. We showcase its effectiveness in healthcare, which is an ideal setting for our method; computational resources are scarce, patient data are ample, and performance is crucial.

Impact Statement

This paper presents work whose goal is to advance the field of Machine Learning. There are many potential societal consequences of our work, none which we feel must be specifically highlighted here.

References

- Arevalo, J., Solorio, T., y Gómez, M. M., and González, F. A. Gated multimodal units for information fusion, 2017. URL <https://arxiv.org/abs/1702.01992>.
- BehnamGhader, P., Adlakha, V., Mosbach, M., Bahdanau, D., Chapados, N., and Reddy, S. Llm2vec: Large language models are secretly powerful text encoders, 2024. URL <https://arxiv.org/abs/2404.05961>.
- Brown, T. B. Language models are few-shot learners. *arXiv preprint arXiv:2005.14165*, 2020.
- Bubeck, S., Chandrasekaran, V., Eldan, R., Gehrke, J., Horvitz, E., Kamar, E., Lee, P., Lee, Y. T., Li, Y., Lundberg, S., et al. Sparks of artificial general intelligence: Early experiments with gpt-4. *arXiv preprint arXiv:2303.12712*, 2023.
- Carballo, K. V., Na, L., Ma, Y., Boussioux, L., Zeng, C., Soenksen, L. R., and Bertsimas, D. Tabtext: A flexible and contextual approach to tabular data representation, 2023. URL <https://arxiv.org/abs/2206.10381>.
- Caron, M., Misra, I., Mairal, J., Goyal, P., Bojanowski, P., and Joulin, A. Unsupervised learning of visual features by contrasting cluster assignments. In *Advances in Neural Information Processing Systems*, volume 33, pp. 9912–9924. Curran Associates, Inc. URL https://papers.neurips.cc/paper_files/paper/2020/hash/70feb62b69f16e0238f741fab228fec2-Abstract.html.
- Chen, T., Kornblith, S., Norouzi, M., and Hinton, G. A simple framework for contrastive learning of visual representations. URL <http://arxiv.org/abs/2002.05709>.
- Devlin, J., Chang, M.-W., Lee, K., and Toutanova, K. Bert: Pre-training of deep bidirectional transformers for language understanding, 2019. URL <https://arxiv.org/abs/1810.04805>.
- Dosovitskiy, A. An image is worth 16x16 words: Transformers for image recognition at scale. *arXiv preprint arXiv:2010.11929*, 2020.
- Dosovitskiy, A., Beyer, L., Kolesnikov, A., Weissenborn, D., Zhai, X., Unterthiner, T., Dehghani, M., Minderer, M., Heigold, G., Gelly, S., Uszkoreit, J., and Houshby, N. An image is worth 16x16 words: Transformers for image recognition at scale, 2021. URL <https://arxiv.org/abs/2010.11929>.
- Dubey, A., Jauhri, A., Pandey, A., Kadian, A., Al-Dahle, A., Letman, A., Mathur, A., Schelten, A., Yang, A., Fan, A., Goyal, A., Hartshorn, A., Yang, A., Mitra, A., Sravankumar, A., Korenev, A., Hinsvark, A., Rao, A., Zhang, A., Rodriguez, A., Gregerson, A., Spataru, A., Roziere, B., Biron, B., Tang, B., Chern, B., Caucheteux, C., Nayak, C., Bi, C., Marra, C., McConnell, C., Keller, C., Touret, C., Wu, C., Wong, C., Ferrer, C. C., Nikolaidis, C., Al-lonsius, D., Song, D., Pintz, D., Livshits, D., Esiobu, D., Choudhary, D., Mahajan, D., Garcia-Olano, D., Perino, D., Hupkes, D., Lakomkin, E., AlBadawy, E., Lobanova, E., Dinan, E., Smith, E. M., Radenovic, F., Zhang, F., Synnaeve, G., Lee, G., Anderson, G. L., Nail, G., Mialon, G., Pang, G., Cucurell, G., Nguyen, H., Korevaar, H., Xu, H., Touvron, H., Zarov, I., Ibarra, I. A., Kloumann, I., Misra, I., Evtimov, I., Copet, J., Lee, J., Geffert, J., Vranes, J., Park, J., Mahadeokar, J., Shah, J., van der Linde, J., Billock, J., Hong, J., Lee, J., Fu, J., Chi, J., Huang, J., Liu, J., Wang, J., Yu, J., Bitton, J., Spisak, J., Park, J., Rocca, J., Johnstun, J., Saxe, J., Jia, J., Alwala, K. V., Upasani, K., Plawiak, K., Li, K., Heafield, K., Stone, K., El-Arini, K., Iyer, K., Malik, K., Chiu, K., Bhalla, K., Rantala-Yeary, L., van der Maaten, L., Chen, L., Tan, L., Jenkins, L., Martin, L., Madaan, L., Malo, L., Blecher, L., Landzaat, L., de Oliveira, L., Muzzi, M., Pasupuleti, M., Singh, M., Paluri, M., Kardas, M., Oldham, M., Rita, M., Pavlova, M., Kambadur, M., Lewis, M., Si, M., Singh, M. K., Hassan, M., Goyal, N., Torabi, N., Bashlykov, N., Bogoychev, N., Chatterji, N., Duchenne, O., Çelebi, O., Alrassy, P., Zhang, P., Li, P., Vasic, P., Weng, P., Bhargava, P., Dubal, P., Krishnan, P., Koura, P. S., Xu, P., He, Q., Dong, Q., Srinivasan, R., Ganapathy, R., Calderer, R., Cabral, R. S., Stojnic, R., Raileanu, R., Girdhar, R., Patel, R., Sauvestre, R., Polidoro, R., Sumbaly, R., Taylor, R., Silva, R., Hou, R., Wang, R., Hosseini, S., Chennabasappa, S., Singh, S., Bell, S., Kim, S. S., Edunov, S., Nie, S., Narang, S., Raparthy, S., Shen, S., Wan, S., Bhosale, S., Zhang, S., Vandenhende, S., Batra, S., Whitman, S., Sootla, S., Collot, S., Gururangan, S., Borodinsky, S., Herman, T., Fowler, T., Sheasha, T., Georgiou, T., Scialom, T., Speckbacher, T., Mihaylov, T., Xiao, T., Karn, U., Goswami, V., Gupta, V., Ramanathan, V., Kerkez, V., Gonguet, V., Do, V., Vogeti, V., Petrovic, V., Chu, W., Xiong, W., Fu, W., Meers, W., Martinet, X., Wang, X., Tan, X. E., Xie, X., Jia, X., Wang, X., Goldschlag, Y., Gaur, Y., Babaei, Y., Wen, Y., Song, Y., Zhang, Y., Li, Y., Mao, Y., Coudert, Z. D., Yan, Z., Chen, Z., Papakipos, Z., Singh, A., Grattafiori, A., Jain, A., Kelsey, A., Shajnfeld, A., Gangidi, A., Victoria, A., Goldstand, A., Menon, A., Sharma, A., Boesenberg, A., Vaughan, A., Baevski, A., Feinstein, A., Kallet, A., Sangani, A., Yunus, A., Lupu, A., Alvarado, A., Caples, A., Gu, A., Ho, A., Poulton, A., Ryan, A., Ramchandani, A., Franco, A., Saraf, A., Chowdhury, A., Gabriel, A., Bharambe, A., Eisenman, A.,

- Yazdan, A., James, B., Maurer, B., Leonhardi, B., Huang, B., Loyd, B., Paola, B. D., Paranjape, B., Liu, B., Wu, B., Ni, B., Hancock, B., Wasti, B., Spence, B., Stojkovic, B., Gamido, B., Montalvo, B., Parker, C., Burton, C., Mejia, C., Wang, C., Kim, C., Zhou, C., Hu, C., Chu, C.-H., Cai, C., Tindal, C., Feichtenhofer, C., Civin, D., Beaty, D., Kreymer, D., Li, D., Wyatt, D., Adkins, D., Xu, D., Testuggine, D., David, D., Parikh, D., Liskovich, D., Foss, D., Wang, D., Le, D., Holland, D., Dowling, E., Jamil, E., Montgomery, E., Presani, E., Hahn, E., Wood, E., Brinkman, E., Arcaute, E., Dunbar, E., Smothers, E., Sun, F., Kreuk, F., Tian, F., Ozgenel, F., Caggioni, F., Guzmán, F., Kanayet, F., Seide, F., Florez, G. M., Schwarz, G., Badeer, G., Swee, G., Halpern, G., Thattai, G., Herman, G., Sizov, G., Guangyi, Zhang, Lakshminarayanan, G., Shojanazeri, H., Zou, H., Wang, H., Zha, H., Habeeb, H., Rudolph, H., Suk, H., Aspegren, H., Goldman, H., Damlaj, I., Molybog, I., Tufanov, I., Veliche, I.-E., Gat, I., Weissman, J., Geboski, J., Kohli, J., Asher, J., Gaya, J.-B., Marcus, J., Tang, J., Chan, J., Zhen, J., Reizenstein, J., Teboul, J., Zhong, J., Jin, J., Yang, J., Cummings, J., Carvill, J., Shepard, J., McPhie, J., Torres, J., Ginsburg, J., Wang, J., Wu, K., U, K. H., Saxena, K., Prasad, K., Khandelwal, K., Zand, K., Matosich, K., Veeraraghavan, K., Michelena, K., Li, K., Huang, K., Chawla, K., Lakhota, K., Huang, K., Chen, L., Garg, L., A, L., Silva, L., Bell, L., Zhang, L., Guo, L., Yu, L., Moshkovich, L., Wehrstedt, L., Khabsa, M., Avalani, M., Bhatt, M., Tsimpoukelli, M., Mankus, M., Hasson, M., Lennie, M., Reso, M., Groshev, M., Naumov, M., Lathi, M., Kenally, M., Seltzer, M. L., Valko, M., Restrepo, M., Patel, M., Vyatskov, M., Samvelyan, M., Clark, M., Macey, M., Wang, M., Hermoso, M. J., Metanat, M., Rastegari, M., Bansal, M., Santhanam, N., Parks, N., White, N., Bawa, N., Singhal, N., Egebo, N., Usunier, N., Laptev, N. P., Dong, N., Zhang, N., Cheng, N., Chernoguz, O., Hart, O., Salpekar, O., Kalinli, O., Kent, P., Parekh, P., Saab, P., Balaji, P., Rittner, P., Bontrager, P., Roux, P., Dollar, P., Zvyagina, P., Ratanchandani, P., Yuvraj, P., Liang, Q., Alao, R., Rodriguez, R., Ayub, R., Murthy, R., Nayani, R., Mitra, R., Li, R., Hogan, R., Battey, R., Wang, R., Maheswari, R., Howes, R., Rinott, R., Bondu, S. J., Datta, S., Chugh, S., Hunt, S., Dhillon, S., Sidorov, S., Pan, S., Verma, S., Yamamoto, S., Ramaswamy, S., Lindsay, S., Lindsay, S., Feng, S., Lin, S., Zha, S. C., Shankar, S., Zhang, S., Zhang, S., Wang, S., Agarwal, S., Sajuyigbe, S., Chintala, S., Max, S., Chen, S., Kehoe, S., Satterfield, S., Govindaprasad, S., Gupta, S., Cho, S., Virk, S., Subramanian, S., Choudhury, S., Goldman, S., Remez, T., Glaser, T., Best, T., Kohler, T., Robinson, T., Li, T., Zhang, T., Matthews, T., Chou, T., Shaked, T., Vontimitta, V., Ajayi, V., Montanez, V., Mohan, V., Kumar, V. S., Mangla, V., Albiero, V., Ionescu, V., Poenaru, V., Mihailescu, V. T., Ivanov, V., Li, W., Wang, W., Jiang, W., Bouaziz, W., Constable, W., Tang, X., Wang, X., Wu, X., Wang, X., Xia, X., Wu, X., Gao, X., Chen, Y., Hu, Y., Jia, Y., Qi, Y., Li, Y., Zhang, Y., Zhang, Y., Adi, Y., Nam, Y., Yu, Wang, Hao, Y., Qian, Y., He, Y., Rait, Z., DeVito, Z., Rosnbrick, Z., Wen, Z., Yang, Z., and Zhao, Z. The llama 3 herd of models, 2024. URL <https://arxiv.org/abs/2407.21783>.
- Gutmann, M. and Hyvärinen, A. Noise-contrastive estimation: A new estimation principle for unnormalized statistical models. In *Proceedings of the Thirteenth International Conference on Artificial Intelligence and Statistics*, pp. 297–304. JMLR Workshop and Conference Proceedings. URL <https://proceedings.mlr.press/v9/gutmann10a.html>. ISSN: 1938-7228.
- He, K., Fan, H., Wu, Y., Xie, S., and Girshick, R. Momentum contrast for unsupervised visual representation learning. In *2020 IEEE/CVF Conference on Computer Vision and Pattern Recognition (CVPR)*, pp. 9726–9735. IEEE. ISBN 978-1-72817-168-5. doi: 10.1109/CVPR42600.2020.00975. URL <https://ieeexplore.ieee.org/document/9157636/>.
- Healthcare Cost and Utilization Project (HCUP). *Introduction to the HCUP National Inpatient Sample (NIS)*. Agency for Healthcare Research and Quality, Rockville, MD, Jun 2021. URL https://www.hcup-us.ahrq.gov/db/nation/nis/NIS_Introduction_2018.jsp. The National (Nationwide) Inpatient Sample database documentation.
- Huang, K., Altonaar, J., and Ranganath, R. Clinicalbert: Modeling clinical notes and predicting hospital readmission. *arXiv preprint arXiv:1904.05342*, 2019.
- Jia, C., Yang, Y., Xia, Y., Chen, Y.-T., Parekh, Z., Pham, H., Le, Q. V., Sung, Y., Li, Z., and Duerig, T. Scaling up visual and vision-language representation learning with noisy text supervision. URL <http://arxiv.org/abs/2102.05918>.
- Li, Z., Zhang, X., Zhang, Y., Long, D., Xie, P., and Zhang, M. Towards general text embeddings with multi-stage contrastive learning, 2023. URL <https://arxiv.org/abs/2308.03281>.
- Mikolov, T. Efficient estimation of word representations in vector space. *arXiv preprint arXiv:1301.3781*, 2013.
- Muennighoff, N., Tazi, N., Magne, L., and Reimers, N. Mteb: Massive text embedding benchmark, 2023. URL <https://arxiv.org/abs/2210.07316>.
- Oord, A. v. d., Li, Y., and Vinyals, O. Representation learning with contrastive predictive coding. URL <http://arxiv.org/abs/1807.03748>.

- Oquab, M., Darcet, T., Moutakanni, T., Vo, H., Szafraniec, M., Khalidov, V., Fernandez, P., Haziza, D., Massa, F., El-Nouby, A., et al. Dinov2: Learning robust visual features without supervision. *arXiv preprint arXiv:2304.07193*, 2023.
- Oquab, M., Darcet, T., Moutakanni, T., Vo, H., Szafraniec, M., Khalidov, V., Fernandez, P., Haziza, D., Massa, F., El-Nouby, A., Assran, M., Ballas, N., Galuba, W., Howes, R., Huang, P.-Y., Li, S.-W., Misra, I., Rabbat, M., Sharma, V., Synnaeve, G., Xu, H., Jegou, H., Mairal, J., Labatut, P., Joulin, A., and Bojanowski, P. Dinov2: Learning robust visual features without supervision, 2024. URL <https://arxiv.org/abs/2304.07193>.
- Radford, A., Kim, J. W., Hallacy, C., Ramesh, A., Goh, G., Agarwal, S., Sastry, G., Askell, A., Mishkin, P., Clark, J., Krueger, G., and Sutskever, I. Learning transferable visual models from natural language supervision. URL <http://arxiv.org/abs/2103.00020>.
- Radford, A., Kim, J. W., Hallacy, C., Ramesh, A., Goh, G., Agarwal, S., Sastry, G., Askell, A., Mishkin, P., Clark, J., et al. Learning transferable visual models from natural language supervision. In *International conference on machine learning*, pp. 8748–8763. PMLR, 2021.
- Soenksen, L. R., Ma, Y., Zeng, C., Boussioux, L., Vilalobos Carballo, K., Na, L., Wiberg, H. M., Li, M. L., Fuentes, I., and Bertsimas, D. Integrated multimodal artificial intelligence framework for healthcare applications. *npj Digital Medicine*, 5(1):149, Sep 2022. ISSN 2398-6352. doi: 10.1038/s41746-022-00689-4. URL <https://doi.org/10.1038/s41746-022-00689-4>.
- Xia, M., Wilson, J., Goldstein, B., and Henao, R. Contrastive learning for clinical outcome prediction with partial data sources. In *Forty-first International Conference on Machine Learning*.
- Yang, A., Yang, B., Hui, B., Zheng, B., Yu, B., Zhou, C., Li, C., Li, C., Liu, D., Huang, F., Dong, G., Wei, H., Lin, H., Tang, J., Wang, J., Yang, J., Tu, J., Zhang, J., Ma, J., Yang, J., Xu, J., Zhou, J., Bai, J., He, J., Lin, J., Dang, K., Lu, K., Chen, K., Yang, K., Li, M., Xue, M., Ni, N., Zhang, P., Wang, P., Peng, R., Men, R., Gao, R., Lin, R., Wang, S., Bai, S., Tan, S., Zhu, T., Li, T., Liu, T., Ge, W., Deng, X., Zhou, X., Ren, X., Zhang, X., Wei, X., Ren, X., Liu, X., Fan, Y., Yao, Y., Zhang, Y., Wan, Y., Chu, Y., Liu, Y., Cui, Z., Zhang, Z., Guo, Z., and Fan, Z. Qwen2 technical report, 2024. URL <https://arxiv.org/abs/2407.10671>.
- Zhang, Y., Jiang, H., Miura, Y., Manning, C. D., and Langlotz, C. P. Contrastive learning of medical visual representations from paired images and text. URL <http://arxiv.org/abs/2010.00747>.

A. Additional Results

A.1. Summary Results

In Table (2), (7) and (8), we show the average F1, AUC and Accuracy scores across all models and feature extractors for each projection method and dataset. Then, In table (9), (10) and (11), we show the best F1, AUC and Accuracy between all models and feature extractors for each projection method and task.

Table 7: Average AUC Score (%) Across Experiments

METHOD	DIABETES	HYPERTENSION	MOVIES
UNPROJECTED	78.0 (± 15.0)	66.8 (± 10.9)	79.6 (± 16.5)
SINGLE PROJ (CONTR.)	79.1 (± 14.2)	65.4 (± 8.5)	82.4 (± 14.2)
SINGLE PROJ (PCA)	74.6 (± 15.2)	64.1 (± 9.3)	80.4 (± 16.0)
PER-MOD (CONTR.)	86.9 (± 5.8)	68.5 (± 8.5)	87.7 (± 5.1)
PER-MOD (PCA)	77.0 (± 16.1)	65.2 (± 9.9)	79.6 (± 16.6)

VALUES SHOW MEAN AUC SCORES & STANDARD DEVIATIONS ACROSS ALL MODELS AND FEATURE EXTRACTORS

Table 8: Average Accuracy Score (%) Across Experiments

METHOD	DIABETES	HYPERTENSION	MOVIES
UNPROJECTED	77.1 (± 8.5)	83.2 (± 3.5)	78.2 (± 7.9)
SINGLE PROJ (CONTR.)	78.7 (± 7.2)	83.1 (± 1.7)	81.5 (± 6.1)
SINGLE PROJ (PCA)	74.3 (± 8.2)	82.8 (± 3.1)	79.5 (± 7.5)
PER-MOD (CONTR.)	84.4 (± 3.5)	84.5 (± 2.3)	85.0 (± 1.6)
PER-MOD (PCA)	76.3 (± 8.7)	83.1 (± 3.3)	77.9 (± 8.1)

VALUES SHOW MEAN ACCURACY SCORES & STANDARD DEVIATIONS ACROSS ALL MODELS AND FEATURE EXTRACTORS

Table 9: Best F1 Score (%) Across Experiments

METHOD	DIABETES		HYPERTENSION		MOVIES	
	F1	MODEL	F1	MODEL	F1	MODEL
UNPROJECTED	81.2	LR	35.5	LR	77.9	MLP
SINGLE PROJ (CONTR.)	79.2	LR	31.4	MLP	76.9	LR
SINGLE PROJ (PCA)	79.3	LR	29.3	MLP	79.2	LR
PER-MOD (CONTR.)	82.5	LR	32.5	XGB	77.4	LR
PER-MOD (PCA)	79.9	LR	38.4	LR	79.2	MLP

MODELS – **LR**: LOGISTIC REGRESSION, **RF**: RANDOM FOREST
EMBEDDINGS – **MOVIES**: BERT+ViT; **CLINICAL TASKS**: CLINICALBERT

Table 11: Best Accuracy (%) Across Experiments

METHOD	DIABETES		HYPERTENSION		MOVIES	
	ACC	MODEL	ACC	MODEL	ACC	MODEL
UNPROJECTED	87.5	LR	86.0	XGB	85.6	MLP
SINGLE PROJ (CONTR.)	86.1	XGB	85.2	SVC	84.9	LR
SINGLE PROJ (PCA)	86.3	LR	85.2	LR	86.7	LR
PER-MOD (CONTR.)	88.4	LR	86.2	SVC	85.7	RF
PER-MOD (PCA)	86.6	MLP	85.2	XGB	86.5	MLP

MODELS – **LR**: LOGISTIC REGRESSION, **RF**: RANDOM FOREST
EMBEDDINGS – **MOVIES**: BERT+ViT; **CLINICAL TASKS**: CLINICALBERT

Table 10: Best AUC Score (%) Across Tasks

METHOD	DIABETES		HYPERTENSION		MOVIES	
	AUC	MODEL	AUC	MODEL	AUC	MODEL
UNPROJECTED	92.9	LR	76.7	LR	91.9	LR
SINGLE PROJ (CONTR.)	91.4	LR	73.4	LR	91.4	LR
SINGLE PROJ (PCA)	91.4	LR	74.9	LR	92.8	LR
PER-MOD (CONTR.)	93.7	LR	76.3	LR	91.6	LR
PER-MOD (PCA)	92.5	MLP	75.5	LR	92.4	MLP

MODELS – **LR**: LOGISTIC REGRESSION, **RF**: RANDOM FOREST
EMBEDDINGS – **MOVIES**: BERT+ViT; **CLINICAL TASKS**: CLINICALBERT

A.2. Detailed Breakdown of Unprojected Results

In table (12), we show the performance of the unprojected embeddings across all tasks and models. This serves as the baseline for the other methods, from which we calculate the Δ of the performance of the other methods.

Table 12: Baseline (Unprojected) Performance Across All Tasks and Models

TASK	EXTRACTOR	MODEL	F1 (%)	AUC (%)	ACC (%)
DIABETES	CLINICALBERT	CART	55.9 (± 2.2)	66.2 (± 1.5)	69.0 (± 1.1)
		LR	81.2 (± 2.0)	92.9 (± 0.9)	87.5 (± 1.0)
		MLP	79.7 (± 2.2)	91.6 (± 0.9)	86.4 (± 1.3)
		SVC	0.1 (± 0.0)	50.0 (± 0.0)	65.4 (± 2.4)
		XGB	74.4 (± 1.6)	90.5 (± 1.2)	84.4 (± 0.9)
	GTE+QWEN2	CART	45.9 (± 2.1)	58.7 (± 1.4)	62.5 (± 1.4)
		LR	59.2 (± 1.6)	84.1 (± 0.5)	77.6 (± 1.4)
		MLP	69.0 (± 1.2)	85.0 (± 0.4)	79.8 (± 0.8)
		SVC	26.6 (± 4.6)	57.3 (± 1.6)	70.0 (± 3.1)
		XGB	59.3 (± 1.4)	82.9 (± 0.7)	76.9 (± 2.3)
HYPERTENSION	CLINICALBERT	CART	26.3 (± 3.3)	56.7 (± 2.1)	77.1 (± 1.6)
		LR	35.5 (± 1.8)	76.7 (± 2.5)	85.0 (± 0.9)
		MLP	35.0 (± 4.2)	74.3 (± 2.6)	83.0 (± 1.1)
		SVC	0.1 (± 0.0)	50.0 (± 0.0)	85.1 (± 1.3)
		XGB	21.1 (± 4.8)	75.3 (± 2.8)	86.0 (± 1.4)
	GTE+QWEN2	CART	17.2 (± 3.7)	51.4 (± 1.8)	75.3 (± 1.0)
		LR	2.7 (± 2.2)	74.3 (± 1.2)	85.2 (± 1.4)
		MLP	28.9 (± 4.1)	73.5 (± 1.5)	84.3 (± 1.5)
		SVC	0.1 (± 0.0)	50.0 (± 0.0)	85.1 (± 1.3)
		XGB	6.9 (± 2.4)	71.5 (± 1.0)	85.0 (± 1.1)
MOVIES	BERT+ViT	CART	53.5 (± 3.4)	65.1 (± 2.1)	68.8 (± 1.8)
		LR	77.4 (± 0.3)	91.9 (± 0.4)	85.3 (± 0.5)
		MLP	77.9 (± 2.9)	91.9 (± 0.4)	85.6 (± 1.8)
		RF	56.4 (± 3.2)	87.8 (± 0.8)	78.8 (± 1.3)
		SVC	0.3 (± 0.4)	50.1 (± 0.1)	66.9 (± 1.3)
XGB	72.1 (± 1.5)	90.5 (± 0.7)	83.5 (± 0.6)		

ALL METRICS ARE IN PERCENTAGES (%)
LR: LOGISTIC REGRESSION, RF: RANDOM FOREST, XGB: XGBOOST
STANDARD DEVIATIONS SHOWN IN PARENTHESES

A.3. Detailed Breakdown of Results

In this section, we provide detailed breakdowns of model performance using additional metrics beyond F1 score. For each dataset, we show the Δ of both accuracy (tables 13, 14, 15) and AUC (tables 16, 17, 18) improvements over the baseline (unprojected) method, which is reported in table (12).

Table 13: Δ Accuracy (%) for *diabetes* with each projection method. Values show differences from unprojected baseline. Best results are shown in **bold**.

EXTR.	MODEL	SINGLE PROJ.		PER-MOD. PROJ.	
		CONTR.	PCA	CONTR.	PCA
CBERT	CART	+13.4 (± 1.9)	-4.8 (± 2.4)	+13.0 (± 0.9)	-1.6 (± 1.8)
CBERT	LR	-1.9 (± 0.7)	-1.4 (± 1.1)	+0.1 (± 1.2)	-1.1 (± 1.2)
CBERT	MLP	-1.1 (± 1.0)	-2.7 (± 1.1)	+1.2 (± 1.4)	+0.1 (± 0.7)
CBERT	SVC	+1.7 (± 2.8)	+0.0 (± 2.4)	+22.6 (± 1.0)	+0.0 (± 2.4)
CBERT	XGB	+1.5 (± 0.5)	-4.1 (± 1.8)	+3.3 (± 1.4)	-0.6 (± 1.0)
GQW	CART	+11.4 (± 1.3)	+0.1 (± 1.9)	+14.7 (± 1.4)	+1.2 (± 2.2)
GQW	LR	-0.6 (± 1.1)	+0.7 (± 1.8)	+3.8 (± 1.0)	+2.3 (± 0.9)
GQW	MLP	-2.2 (± 1.5)	-4.3 (± 1.6)	+2.0 (± 1.0)	-1.0 (± 1.3)
GQW	SVC	-4.7 (± 2.4)	-4.7 (± 2.4)	+11.2 (± 0.9)	-4.7 (± 2.4)
GQW	XGB	+0.5 (± 1.4)	-3.4 (± 1.6)	+4.6 (± 1.5)	+0.1 (± 1.0)

EXTRACTORS – CBERT: CLINICALBERT, GQW: GTE+QWEN2
 MODELS – LR: LOG. REGRESSION, RF: RANDOM FOREST

Table 14: Δ Accuracy (%) for *hypertension* with each projection method. Values show differences from unprojected baseline. Best results are shown in **bold**.

EXTR.	MODEL	SINGLE PROJ.		PER-MOD. PROJ.	
		CONTR.	PCA	CONTR.	PCA
CBERT	CART	+2.8 (± 0.6)	+0.0 (± 1.2)	+1.2 (± 1.5)	+0.1 (± 0.7)
CBERT	LR	-2.1 (± 0.9)	+0.1 (± 0.9)	+0.9 (± 0.9)	-0.5 (± 1.2)
CBERT	MLP	+0.2 (± 0.9)	+0.5 (± 0.8)	+2.0 (± 0.9)	+2.1 (± 1.3)
CBERT	SVC	+0.1 (± 1.1)	+0.0 (± 1.3)	+0.7 (± 1.3)	+0.0 (± 1.3)
CBERT	XGB	-2.6 (± 0.7)	-1.0 (± 1.2)	-1.6 (± 0.9)	-0.5 (± 0.9)
GQW	CART	+4.3 (± 1.7)	+3.6 (± 1.5)	+7.4 (± 0.7)	+2.8 (± 1.3)
GQW	LR	-2.5 (± 1.1)	-0.3 (± 1.0)	-0.2 (± 1.2)	-1.6 (± 1.4)
GQW	MLP	-1.0 (± 1.1)	-2.3 (± 1.4)	+1.2 (± 1.0)	-1.5 (± 1.2)
GQW	SVC	+6.0 (± 1.3)	+0.0 (± 1.3)	-0.2 (± 0.8)	+0.0 (± 1.3)
GQW	XGB	-1.6 (± 1.1)	+0.1 (± 1.5)	-0.2 (± 0.8)	+0.0 (± 1.2)

EXTRACTORS – CBERT: CLINICALBERT, GQW: GTE+QWEN2
 MODELS – LR: LOG. REGRESSION, RF: RANDOM FOREST

Table 15: Δ Accuracy (%) for *movies* with each projection method. Values show differences from unprojected baseline. Best results are shown in **bold**.

EXTR.	MODEL	SINGLE PROJ.		PER-MOD. PROJ.	
		CONTR.	PCA	CONTR.	PCA
BViT	CART	+13.2 (± 1.4)	+3.3 (± 1.1)	+13.7 (± 0.9)	-0.5 (± 0.9)
BViT	LR	-0.3 (± 1.1)	+1.6 (± 0.8)	-0.2 (± 1.6)	+1.2 (± 0.9)
BViT	MLP	-1.1 (± 0.4)	+0.5 (± 0.9)	-0.8 (± 2.2)	+0.5 (± 1.3)
BViT	RF	+6.0 (± 1.1)	+1.3 (± 1.9)	+5.9 (± 1.7)	-4.1 (± 1.3)
BViT	SVC	+5.1 (± 3.6)	+0.0 (± 1.3)	+17.5 (± 1.8)	+0.1 (± 1.3)
BViT	XGB	+0.7 (± 1.3)	+0.8 (± 0.8)	+1.3 (± 1.3)	-0.6 (± 1.3)

EXTRACTORS – BVIT: BERT+ViT MULTIMODAL MODEL
 MODELS – LR: LOG. REGRESSION, RF: RANDOM FOREST

Table 16: Δ AUC (%) for *diabetes* with each projection method. Values show differences from unprojected baseline. Best results are shown in **bold**.

EXTR.	MODEL	SINGLE PROJ.		PER-MOD. PROJ.	
		CONTR.	PCA	CONTR.	PCA
CBERT	CART	+13.9 (± 1.8)	-5.5 (± 2.2)	+14.2 (± 1.3)	-2.5 (± 2.1)
CBERT	LR	-1.6 (± 1.0)	-1.3 (± 0.7)	+0.3 (± 0.6)	-0.9 (± 1.3)
CBERT	MLP	-1.4 (± 0.6)	-2.1 (± 0.9)	+0.4 (± 1.0)	+0.3 (± 1.2)
CBERT	SVC	+2.5 (± 1.4)	+0.0 (± 0.0)	+35.0 (± 1.4)	+0.0 (± 0.0)
CBERT	XGB	+0.4 (± 1.4)	-4.1 (± 1.6)	+1.8 (± 0.9)	-0.8 (± 0.7)
GQW	CART	+12.0 (± 1.3)	-0.4 (± 1.2)	+15.9 (± 1.1)	+1.1 (± 1.9)
GQW	LR	-0.8 (± 1.1)	-0.4 (± 0.9)	+2.8 (± 0.3)	+1.6 (± 0.8)
GQW	MLP	-2.5 (± 1.2)	-5.3 (± 1.4)	+2.2 (± 0.6)	-1.0 (± 0.7)
GQW	SVC	-7.3 (± 0.0)	-7.3 (± 0.0)	+20.1 (± 0.6)	-7.3 (± 0.0)
GQW	XGB	-0.8 (± 0.6)	-6.3 (± 1.6)	+3.5 (± 0.5)	+0.1 (± 1.5)

EXTRACTORS – CBERT: CLINICALBERT, GQW: GTE+QWEN2
 MODELS – LR: LOG. REGRESSION, RF: RANDOM FOREST

Table 17: Δ AUC (%) for *hypertension* with each projection method. Values show differences from unprojected baseline. Best results are shown in **bold**.

EXTR.	MODEL	SINGLE PROJ.		PER-MOD. PROJ.	
		CONTR.	PCA	CONTR.	PCA
CBERT	CART	+2.4 (± 2.4)	-1.5 (± 1.9)	+2.0 (± 1.9)	+0.2 (± 1.4)
CBERT	LR	-4.0 (± 4.0)	-1.8 (± 2.9)	-1.1 (± 2.9)	-0.5 (± 1.7)
CBERT	MLP	-3.6 (± 2.8)	-2.5 (± 3.3)	-1.0 (± 2.3)	+0.8 (± 1.1)
CBERT	SVC	+2.6 (± 0.9)	+0.0 (± 0.0)	+5.2 (± 1.5)	+0.0 (± 0.0)
CBERT	XGB	-6.0 (± 3.3)	-3.8 (± 2.4)	-2.0 (± 2.4)	+0.1 (± 2.8)
GQW	CART	+4.5 (± 1.5)	+2.9 (± 1.2)	+7.9 (± 3.1)	+3.3 (± 2.3)
GQW	LR	-4.0 (± 1.6)	-1.1 (± 1.5)	+0.1 (± 1.8)	-2.9 (± 2.1)
GQW	MLP	-3.1 (± 1.7)	-6.1 (± 1.8)	+2.4 (± 2.3)	-3.9 (± 2.2)
GQW	SVC	+0.0 (± 0.0)	+0.0 (± 0.0)	+1.9 (± 1.2)	+0.0 (± 0.0)
GQW	XGB	-3.1 (± 3.0)	-3.3 (± 2.1)	+0.5 (± 2.1)	-1.6 (± 1.1)

EXTRACTORS – CBERT: CLINICALBERT, GQW: GTE+QWEN2
 MODELS – LR: LOG. REGRESSION, RF: RANDOM FOREST

Table 18: Δ AUC (%) for *movies* with each projection method. Values show differences from unprojected baseline. Best results are shown in **bold**.

EXTR.	MODEL	SINGLE PROJ.		PER-MOD. PROJ.	
		CONTR.	PCA	CONTR.	PCA
BViT	CART	+14.7 (± 1.7)	+3.5 (± 1.5)	+14.6 (± 1.3)	-1.4 (± 1.0)
BViT	LR	-0.5 (± 0.5)	+0.9 (± 0.3)	-0.9 (± 0.9)	+0.3 (± 0.4)
BViT	MLP	-1.1 (± 0.8)	+0.2 (± 0.2)	-1.3 (± 1.3)	+0.6 (± 0.7)
BViT	RF	+1.9 (± 0.6)	-0.7 (± 1.0)	+2.4 (± 0.9)	-1.1 (± 0.4)
BViT	SVC	+8.9 (± 5.3)	+0.0 (± 0.1)	+31.3 (± 2.3)	+0.1 (± 0.0)
BViT	XGB	+0.0 (± 0.9)	+0.1 (± 0.9)	+0.4 (± 0.9)	-0.8 (± 0.5)

EXTRACTORS – BVIT: BERT+ViT MULTIMODAL MODEL
 MODELS – LR: LOG. REGRESSION, RF: RANDOM FOREST